Rise and fall of ice production in the Arctic Ocean's ice factories

S.B. Cornish [1], H.L. Johnson [1], R.D.C. Mallett [2], J. Dörr [3], Y.K. Kostov [4], and A.E. Richards [1]

[1]Department of Earth Sciences, University of Oxford, Oxford, UK
[2]Centre for Polar Observation and Modelling, Earth Sciences, University College London, London, UK
[3]Geophysical Institute, University of Bergen, and Bjerknes Centre for Climate Research, Bergen, Norway
[4]College of Life and Environmental Science, University of Exeter, Exeter, UK

Correspondence: S.B. Cornish (sam.cornish@earth.ox.ac.uk)

Abstract. The volume, extent and age of Arctic sea ice is in decline, yet winter sea ice production appears to have been increasing, despite Arctic warming being most intense during winter months. Several negative feedback processes help to restore Arctic sea ice volume during the winter, though previous work suggests that these mechanisms will be overwhelmed by warming in the future, leading to a fall in ice production. Here, we analyse winter ice production in the Kara and Laptev seas—sometimes referred to as Arctic "ice factories", for their outsized role in supplying the Arctic Ocean with young sea ice. Using the Community Earth System Model's Large Ensemble (CESM-LE), we develop a simple linear model that can explain both the forced rise and forced fall of ice production, in terms of consistent physics. We apply our linear model to observation-based estimates of the same climate variables; our reconstruction of ice production suggests that—just as in CESM-LE—we are currently passing the peak of ice production in the Kara and Laptev seas.

Introduction

Arctic sea ice extent and thickness is in an on-going decline, sustained over at least the length of the satellite record, and directly related to anthropogenic carbon emissions.[1] The retreat of Arctic sea ice is both an expression of and a driver of *Arctic Amplification*, which is the phenomenon of intensified climate change in the Arctic region relative to lower latitudes.[2,3,4] Though losses are observed in all seasons, they are more pronounced during late summer than late winter, in terms of both extent[5] and thickness.[6] These trends reveal that increases in summer melting are to some extent compensated by increasing ice production during winter,[6] though not by enough to prevent the continued decline of the annual mean reservoir of sea ice.

As progressively more ice melts during the summer, winter ice production is critical in restoring the ice pack before the onset of polar day, when the high albedo of sea ice and its snow cover plays a crucial role in the radiative budget of the region. The distribution of sea ice is also important during the winter; it limits heat fluxes from the ocean to atmosphere and plays a complex part in the surface momentum balance.[7] Sea ice growth also plays an important hydrographic role: brine is rejected from sea ice during freezing, and freshwater is redistributed via sea ice motion, which acts as a vector between locations of growth and melt.[8,9]

In this paper, we aim to further understanding of the processes that control winter sea ice production in the Arctic, and explore the competing dynamics of these processes under climate change.

There is an apparent tension in the observation of rising winter sea ice growth in concert with Arctic Amplification, which is intensified during the winter.[3,10] However, the two phenomena are most likely linked.[11] During the autumn and winter, heat sequestered in the Arctic Ocean during the summer is released into the atmosphere prior to and during sea ice growth. Sea ice thinner than ∼0.4 m thick permits heat fluxes one to two orders of magnitude larger than those through perennial ice;[12] thickness declines during winter are an important part of Arctic Amplification, to which Lang et al.[13] attribute a rise of ∼1°C in Arctic surface air temperature per decade. In principle, this surface warming may be partially offset by increased long-wave emission.[14] However, due to the predominantly stable atmospheric stratification, surface warming is inefficiently transmitted to the top of the atmosphere, and therefore outgoing longwave emissions only very weakly compensate the warming (the *lapse-rate feedback*).[15,16,17]

Sea ice growth is inextricably linked to heat fluxes from the ocean to the atmosphere in the Arctic, because growth rate is determined by the energy balance at the lower boundary of the ice, the interface at which ice grows. As ice thickens, the conductive heat loss to the atmosphere declines, and the growth rate slows in direct proportion. Thin ice therefore not only permits higher heat fluxes across it, but also grows more rapidly than thicker ice. This thickness-growth relationship underpins a well-known negative feedback on Arctic sea ice loss.[18,19] There are other effects, however, that also act to promote sea ice growth in a warming Arctic. For one thing, ice that is formed later in the season is more likely to avoid the limiting effects of snow—an effective insulator—on growth rate.[20,21] Similarly, snow melt during summer preconditions more rapid growth at the beginning of the freezing season due to the loss of this insulating snow cover.[22] Additionally, thinner sea ice is weaker and more mobile, leading to an increase in wind-driven sea ice divergence,[23,24,25] which has long been recognised to promote winter growth.[26] These negative feedbacks provide stability to the Arctic sea ice system, such that rapid or irreversible losses for summer sea ice area are unlikely.[27,21,14]

In recent warm winters such as 2015/2016 and 2016/2017, growth suppression and even winter melting have been observed,[28,29,19,30] calling into question whether the action of these negative feedbacks may be becoming overwhelmed by warming. Based on simulations with the sea ice model CICE, Stroeve et al.[19] suggest that the thermodynamic growth during the winter 2016/2017 was 11–13 cm down on the 2011–2017 mean, with the overall positive trend in winter ice growth from 1985 ending in 2012; ice growth then weakens until the end of the model run in 2018. Using the same coupled climate model we employ here (CESM-LE), Petty et al.[31] identify that the positive correlation between temperature and winter growth weakens through the mid-century under the RCP8.5 emissions scenario, eventually becoming a negative relationship—indicative of warming overwhelming the negative feedbacks on sea ice loss.

Observational evidence of increasing winter sea ice production, and model-based suggestions of an imminent or recently-begun decline—both associated with anthropogenic climate change—motivate the questions: when will this transition between rising and falling ice production begin? What physical indicators may help us to predict when we are at this turning point? Building on the recent work of Petty et al. and Stroeve et al., can we understand the changes in ice production in terms of underlying physical processes?

We seek here to answer these questions with a regional focus on the Kara and Laptev seas, a region which has been referred to as the 'ice factory' of the Arctic Ocean[32] (Fig. 1a). Topologically, the Kara and Laptev seas are classified as interior

shelves of the Arctic,[33] and are relatively fresh, receiving 50% of the freshwater runoff to the Arctic Ocean.[34] During winter, winds predominantly drive sea ice northwards from the Siberian coastline in the Kara and Laptev seas (Fig. 1b), opening up perennial flaw leads/polynyas, where open water separates landfast ice from mobile pack ice. Sea ice forms rapidly in these flaw leads, and a number of studies have sought to constrain the outsized contribution to the Arctic sea ice budget made by these regions.[35,36,37,38,39,40] The occurrence of wind patterns that increase the advection of sea ice away from the Siberian coasts thus intensifies sea ice production in these regions, and increases the fraction of (relatively thin) sea ice in the Arctic basin originating in the Kara and Laptev seas.[41,42] High rates of freezing in these shallow seas are also thought to help bolster the cold halocline of the central Arctic basins.[43,44] The stability of the Arctic halocline has emerged as a key climate change indicator,[45] in light of episodic collapses of the winter halocline in the Eurasian basin and northern Barents Sea,[46,47] which lead to the shoaling of Atlantic Waters and increased heat fluxes to the surface.[48]

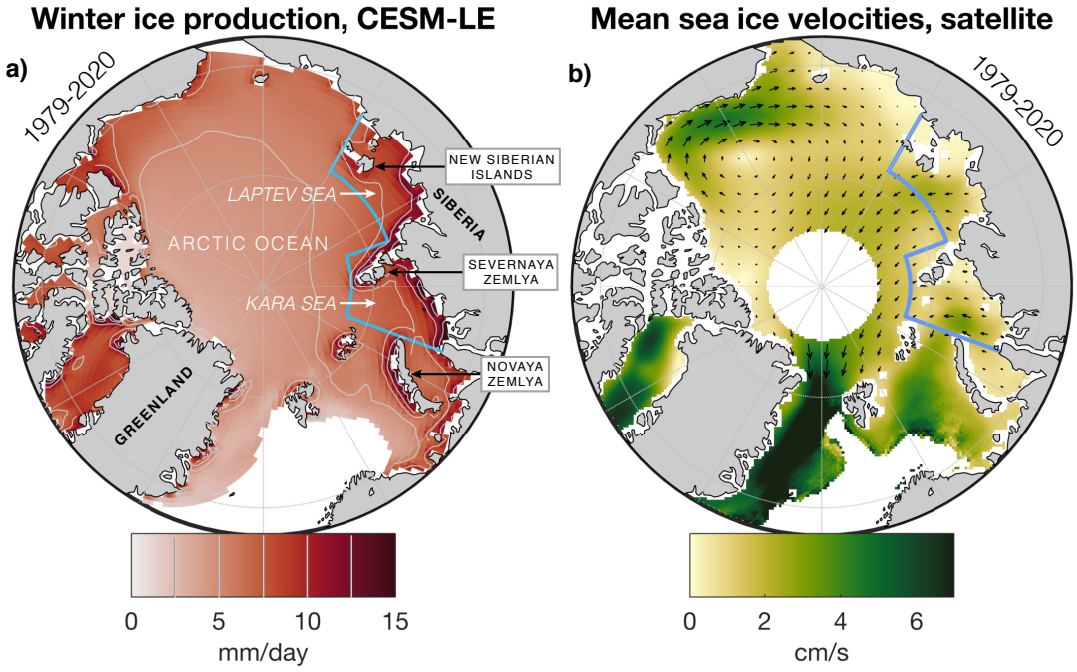

Figure 1. (a) Winter (Oct-Apr) mean ice production for the period 1979–2020 in the ensemble mean of CESM-LE. The Kara and Laptev seas study region is outlined in blue. **(b)** Mean sea ice velocities during 1979–2020 as recorded by the Polar Pathfinder v4.1 product, gridded at 25×25 km resolution and in weekly means.[49] Means taken over periods when sea ice present. Shading indicates the magnitude of the mean velocities. Arrows are omitted in the Barents Sea, Baffin Bay and Greenland Sea, where the colourscale saturates, and flow is generally southwards.

To explain both the rise and fall of sea ice production in the Kara and Laptev seas under climate change, we analyse data from the Large Ensemble of the Community Earth System Model (CESM-LE). We rely on 35 ensemble members and utilise a 20th Century run from 1920–2005 that employs historical external forcing, and a 'high-emissions' RCP8.5 run from 2006–2080.

We develop a simple linear model for ice production that is informed by the physics of sea ice growth, and can successfully explain both the rise and fall of ice production in this region under climate change. We compare the key climate variables from CESM-LE to equivalent variables from a range of observation-based products, and use these variables in our linear model to reconstruct ice production based on this linear model. The reconstruction suggests that, as in CESM-LE, we may presently be passing peak ice production.

Results

Shrinking growth season, rising growth rate

During the summer melt season, large areas of open water develop in the Kara and Laptev seas as the sea ice edge retreats towards the pole (Fig. 2a). The winter refreeze, however, begins along the Siberian coastline.[50] In CESM-LE, the newly formed ice along the Siberian coastline reconnects with the sea ice of the interior Arctic Ocean in an hourglass shape that becomes progressively pinched, and occurs later, through the 21st Century (Fig. 2).

On average, this refreezing in the early winter is the most productive period for winter ice growth (Fig. 3), and is linked to the areal expansion of sea ice (Fig. 2). After an initial peak, ice production in the ensemble mean gradually curtails through the winter—as ice and overlying snow cover thicken—before diminishing more steeply in April. As the climate warms in CESM-LE, however, October ice production rapidly falls, approaching zero by the 2030s (Fig. 3). (Note that ice production as plotted here only considers freezing, and not the negative contribution from melting.) Initially this trend is compensated by a rapid recovery and a higher sea ice production peak in November, connected to the freeze-back of a larger open water area (c.f. Fig. 2). The sea ice production peak itself shifts later after the 2010s, continuing to increase in magnitude until the 2040s, before falling rapidly to mid 20th Century levels by 2080.

The overall trend is one of progressively delayed freezing onset, followed by ice production that is more intense in the mid-winter throughout RCP8.5 than it is in the 20th Century. The graph-area under the ice production curves in Figure 3 represents the total winter ice production; our quantity of interest. In the ensemble mean, ice production rises gently from approximately 1970 to 2010, before falling from 2020 onwards (Fig. 4a).

In examining the causes behind this rise and fall, we start by recognising that sea ice production is limited by the (location-dependent) duration of the freezing season, and the rate of growth where and when it is freezing.

Indeed, we can decompose total ice production into two components (Fig. 4). Firstly, the spatio-temporal duration of freezing, which can be expressed as the number of freezing area days (Fig. 4b). To extend the ice factory metaphor, this can be viewed as the *usage* of the ice factory: the area and time over which it is "switched on". Secondly, we can consider the mean growth rate over the regions where, and times when, sea ice is growing (Fig. 4c). In the ice factory metaphor, this is the *efficiency* of the ice factory when and where it is *in use*. We calculate the mean winter growth rate simply as the total winter ice production divided by the number of freezing area days.

The decomposition reveals quite different trends. The mean number of freezing area days (or *ice factory usage*), begins to decline from the 1990s onwards, which accelerates after 2050 (Fig. 4b). The mean growth rate (or *ice factory efficiency*), on

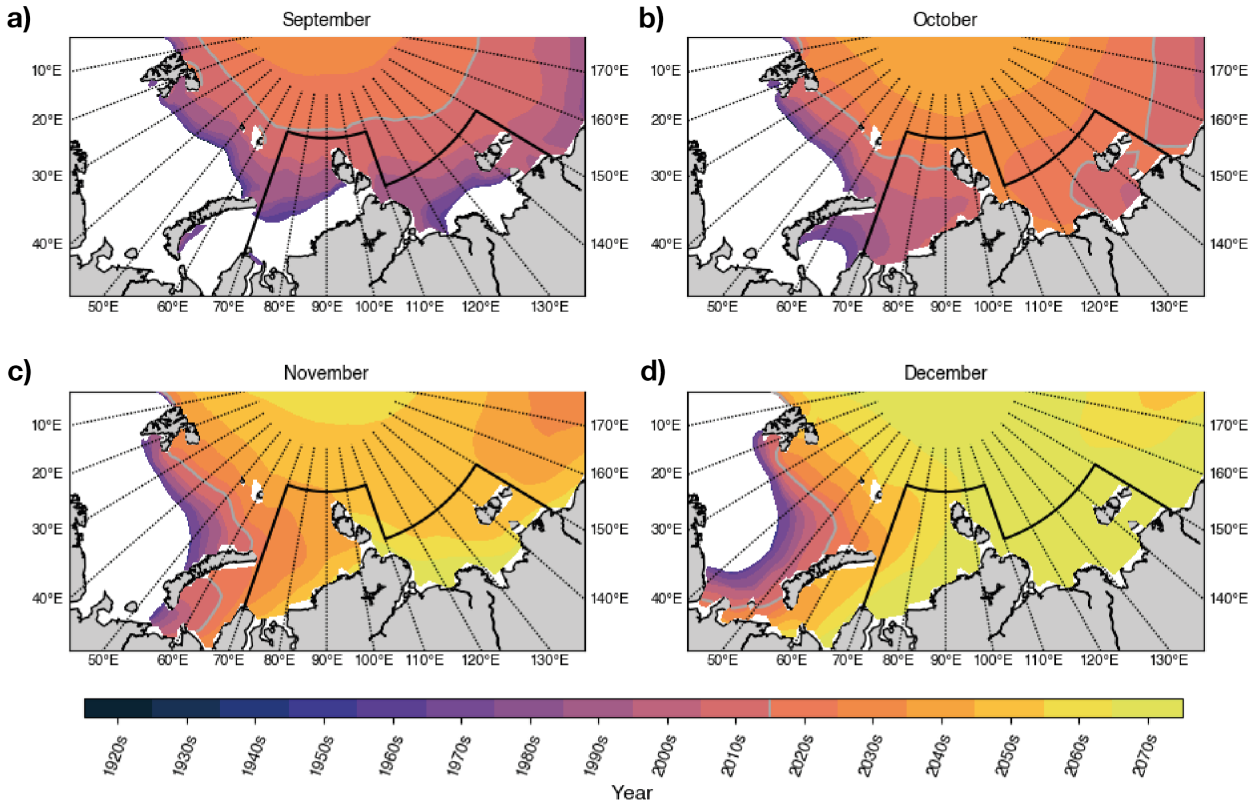

Figure 2. Decadal ensemble mean winter sea ice extent edges in CESM-LE from 1970–2080. Study region outlined in black. Ice edges defined at 15% concentration. Grey line marks the mean 2020s sea ice extent edge.

the other hand, is relatively elevated during the RCP8.5 run in comparison to the 20th Century run (Fig. 4c). Growth rate rises from approximately 1970 to 2030, before declining from approximately 2040 through to 2080.

Physically, the ice factory usage during Oct-Apr is controlled principally by the (location-dependent) time taken to cool the upper ocean to the freezing temperature (approximately -1.8 °C). Heat accumulates in the upper ocean during summer due to penetrating solar radiation, and is sequestered within and often below the mixed layer. In the early winter, ice growth is limited by upwards oceanic heat fluxes as mixing removes heat from the (deepening) mixed layer. A simple regression model, using the mean September surface ocean temperature as a single explanatory variable, captures the internal variability in the number of freezing area days with $R^2 = 0.74$ during the 20th Century run, and with $R^2 = 0.46$ during the RCP8.5 run. The mean surface air temperature during Oct-Dec helps to control the heat flux from ocean to atmosphere as a result of the temperature difference across the ocean-atmosphere interface. Including this climate variable as a second regressor improves the fit in the 20th Century run to $R^2 = 0.78$ and to $R^2 = 0.61$ in the RCP8.5 run.

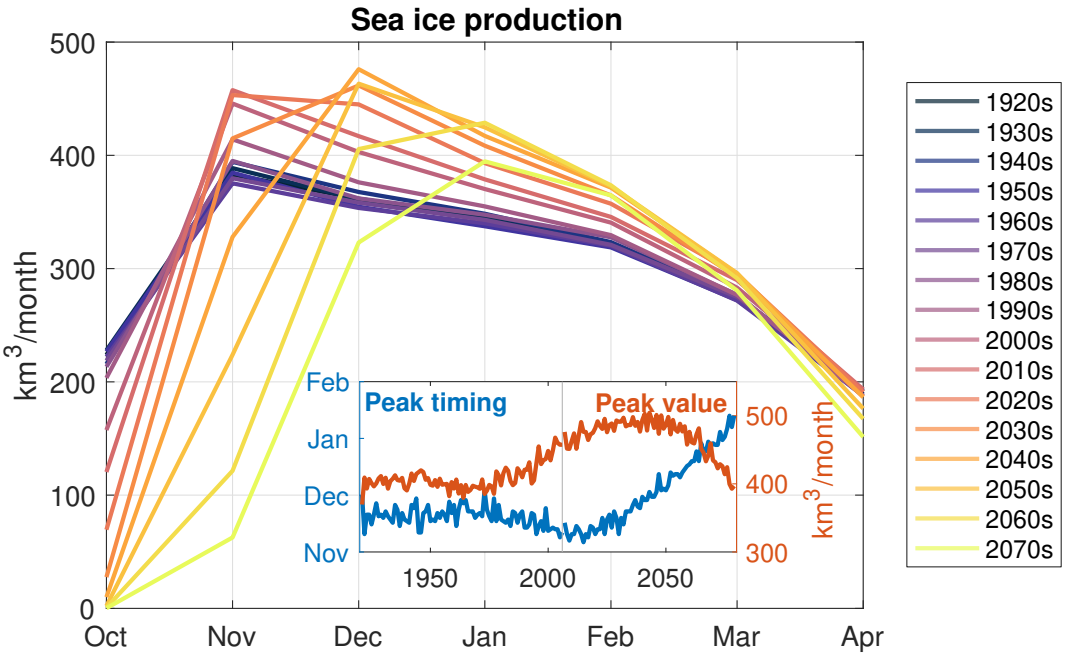

Figure 3. Decadal ensemble mean sea ice production across winter months in CESM-LE. Inset panel shows changes in the timing of peak sea ice production and changes in the amplitude of the peak value. Note that the peak timing is interpolated using the mean of the 35 monthly resolution values from individual ensemble members.

In the absence of incoming shortwave radiation, the growth rate of ice is effectively captured by the balance of heat fluxes at its base.[51] The growth of sea ice, of thickness h_i, depends on a greater conductive heat loss to the atmosphere through the ice, F_c than heat flux from the ocean at its base, F_w, as shown in Equation 1, where ρ_i is the density of ice, L_i is the latent heat release/uptake on freezing/melting, and fluxes are positive upwards.

$$\rho_i L_i \frac{dh_i}{dt} = F_c - F_w \tag{1}$$

As sea ice thickens, the conductive heat fluxes F_c through the ice diminish, bringing the growth rate down towards zero, depending on the size of the oceanic heat flux, F_w. Other factors besides ice thickness also control F_c, including the air temperature and snow cover. Assuming a layer of snow with thickness, h_s overlying ice with thickness, h_i, with corresponding thermal conductivities λ_s and λ_i, respectively, and linear temperature profiles through both layers, the conductive heat flux is

$$F_c = \frac{\Delta T}{\frac{1}{k} + \frac{h_i}{\lambda_i} + \frac{h_s}{\lambda_s}} \tag{2}$$

where k is an effective heat transfer coefficient between the snow/ice surface and the atmosphere, and $\Delta T = T_w - \mathrm{SAT}$; in which T_w is the freezing temperature of water and SAT is the surface atmospheric temperature.

In the Arctic Ocean, F_w is generally low during the freezing season, of order 1 Wm^{-2} or less in the basin interiors, but sometimes higher directly over the Atlantic Water boundary current or over rough topography.[52] Unlike in the Southern Ocean, where F_w is on the order several tens of Wm^{-2}, these low heat fluxes are generally no impediment to the growth of first year ice.[53,51]

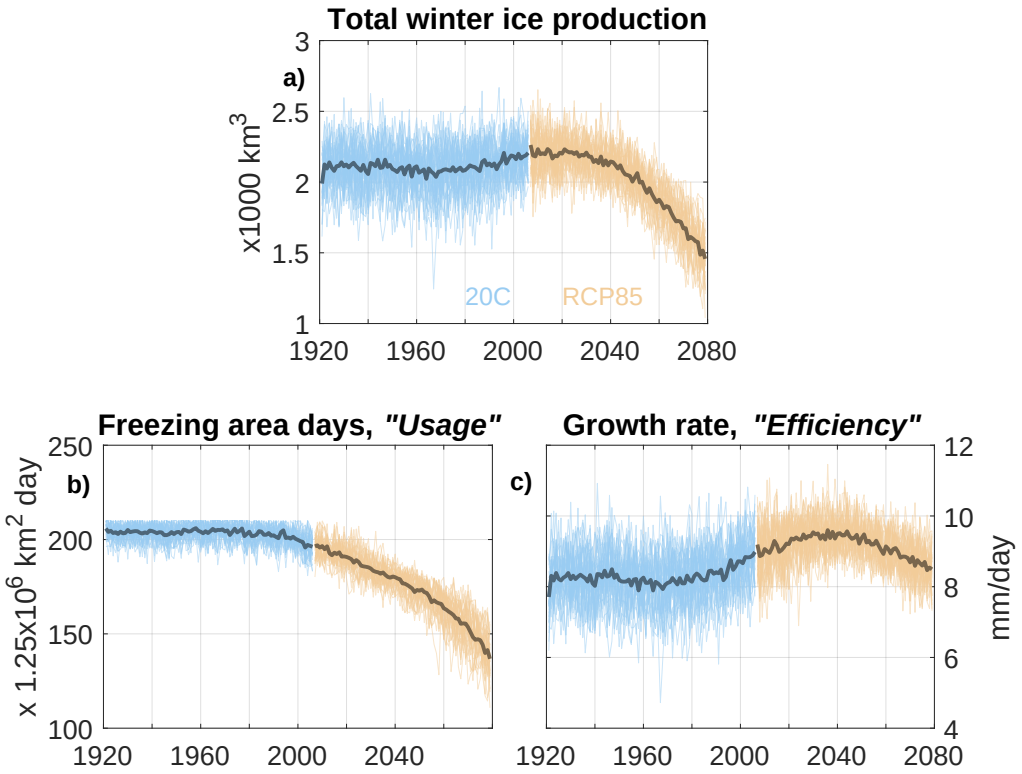

Figure 4. Winter ice production (a) and decomposition into freezing area days (b) and growth rate (c). Note that the freezing area days is rescaled in terms of the total area of the study region, such that the upper limit is 210 on the y axis: the duration of our seven month winter period in days.

A linear model for ice production

By revealing that the number of freezing area days and mean winter growth rate exhibit quite different characteristics, the decomposition in Fig. 4 offers a high-level insight into the competing processes governing ice production changes. We now

seek to isolate a set of observable variables that can capture the physics of these processes. We then explain the changes in ice production through time with a linear model involving these variables.

As discussed above, variability in the number of freezing area days during Oct-Apr is dominantly captured by variation in the Sep sea surface temperature. The mean growth rate, meanwhile, must be controlled by the variables affecting the heat fluxes F_w and F_c (Equation 1). We can diagnose F_w directly from the climate model and observations (though the latter are sparse), but we seek to capture F_c in terms of readily observable climate variables, using insight from Equation 2.

The conductive heat flux is inversely dependent on snow and ice thicknesses (Equation 2). Since snow is much more insulating than ice ($\lambda_s \approx 0.1\lambda_i$), even a thin layer of snow may significantly affect the conductive heat flux.[51] Equation 2 also shows that as surface air temperatures rise—and ΔT lessens—the conductive heat flux decreases in linear relation, as does the growth rate (Equation 1). Positive correlations between surface air temperatures and growth rate[31] rest on a causality in the opposite direction: increased growth rates and attendant upwards heat fluxes serve to boost surface air temperatures. We must therefore include the effect of air temperature in a way that explicitly captures its causal impact on sea ice growth. We do this—as detailed below—by mimicking the growth rate equation, and including ΔT as a factor in each of our regressors.

The sea ice thickness h_i features on both sides of the growth rate equation (Equation 1) due to its involvement in F_c. Therefore, to avoid circular logic we must not include the evolution of h_i in our linear model. However, we can consider initial conditions from which h_i evolves according to the given growth rate. These initial conditions can be both the ice thickness at the start of the season, and occasions during the season when h_i is set to zero (by divergence) as an initial condition for growth. The minimum sea ice area (usually occurring in September) determines the area over which $h_i = 0$ at the start of the season: the September open water area. In addition, open water is created near-continually throughout the freezing season by divergence. Under tension, ice cracks in a brittle manner rather than thinning; the open water area is equal to the area diverged.

Divergence of the Arctic ice pack is spatially and temporally complex, and to understand its effect on thermodynamic growth we must also consider the role of convergence, which thickens ice through ridging and rafting, and may partially balance divergence that occurs in a given area. Because the growth rate of ice is an inverse function of its thickness (Equation 2), and because ice cracks under tension—thus setting h_i = 0 in the diverged area—we can expect the effect of convergence and divergence on growth rate to be asymmetric. Indeed, in grid cells that exhibit both sea ice divergence and freezing within the Kara-Laptev region, divergence explains 37% of the variability in thermodynamic ice growth. In convergent-freezing cells on the other hand, there is no significant relationship. Because the effect of divergence on growth rate is not balanced by the effect of convergence, we must consider not only net divergence over the region, but also divergence that is balanced by convergence elsewhere within the region: we term this the *compensated* divergence. There is, by design, no double-counting between the *net* and *compensated* divergence. The two are therefore only weakly correlated—preferable for the purposes of building a linear model.

We thus classify three settings in which open water is made available for ice growth: the September open water, created by summer melting and ice advection; the open water area due to net divergence; and the open water area due to compensated divergence. The sea ice growth in such open water areas will be linearly related to ΔT and the area that has been opened. In

our linear model, we neglect the timing of divergence and simply use the total area diverged during the winter season in both cases.

We can include the effect of snow as $\Delta T/h_s$, as per Equation 2, where h_s is the mean winter snow depth wherever ice is present. Gathering together these terms, our linear model for total winter ice production, including regression coefficients, β_n is then:

$$\text{Ice Prod} = \beta_1 \Delta T/h_s + \beta_2 \Delta T A_{Sep} + \beta_3 \Delta T A_{net} + \beta_4 \Delta T A_{comp} + \beta_5 \text{SST}_{Sep} \quad (3)$$

Where h_s is the mean snow thickness where ice is present, A_{Sep} is the open water area available in September, A_{net} is the net area diverged integrated over the winter season, A_{comp} is the compensated area diverged integrated over the winter season, SST_{Sep} is the September sea surface temperature (the top 10 m ocean temperature), and ΔT is the temperature difference across the ice, determined by the surface atmospheric temperature only as we set T_w to -1.8 °C (the freezing temperature). We do not include the ocean-to-ice heat flux term, F_w; this is simply because, when included in this multiple regression, it is statistically insignificant.

We perform multiple linear regression across the ensemble members of CESM-LE to determine β_n, using internal variability during a) the 20th Century run, b) the RCP8.5 run and c) the full timeseries (Fig. 5). We plot standardised coefficients, using 20th Century run standard deviation values. This indicates which regressors have the largest effect on ice production in terms of the natural range of variability in the 20th Century run. We preserve this standardisation in the plots for the RCP8.5 run and the full timeseries coefficients in order to compare absolute magnitudes. The variance in the CESM-LE internal variability explained by the linear model is consistently high: 81% during the 20th Century run, 76% during the RCP8.5 run and 78% over the full run.

There is relatively good agreement between the coefficients determined using the 20th Century, RCP8.5 and full timeseries of CESM-LE, and unanimous agreement in the sign. This suggests that the linear model is robust to different climate conditions. The absolute magnitude of the $\Delta T/h_s$ coefficient (β_1)is remarkably similar between runs (Fig. 5). We can estimate the uncertainty associated with these estimates by limiting the dataset to individual ensemble members (grey points, Fig. 5). In the main, individual ensemble members yield estimates that cluster around the full ensemble value. However, for the coefficient associated with September open water $\times \Delta T$ in RCP8.5, the full ensemble value lies outside this range; an effect likely due to September open water area becoming an increasingly skewed variable with time, as it is limited to the total area under consideration.

Three regressors are consistently dominant in their contribution to the internal variability: net divergence $\times \Delta T$, Sep open water $\times \Delta T$, and inverse snow depth $\times \Delta T$. It is worth noting, however, that their role in forced changes in ice production—as given by the ensemble mean—also depends on the magnitude of forced trends in each regressor.

Explaining forced changes in ice production

Having seen that our linear model can explain a large fraction of the internal variability in sea ice production in CESM-LE, we now ask whether it can explain the forced changes in sea ice production associated with climate change (Fig. 6a) and, in

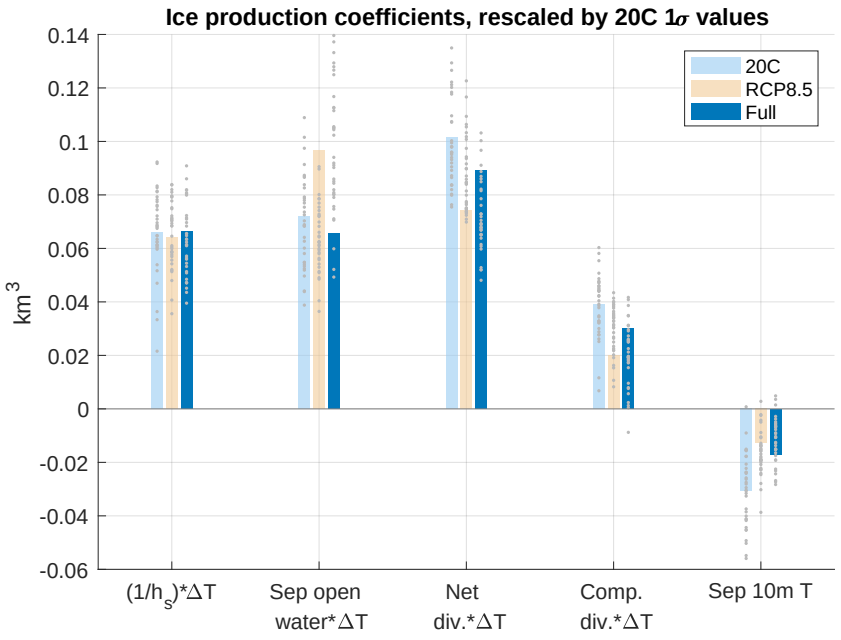

Figure 5. Winter ice production regression coefficients, standardised by the respective one standard deviation values in the 20th Century run. Bars show the regression coefficients calculated using internal variability in all 35 ensemble members, with the ensemble mean removed. Variance explained is as follows. 20C, $R^2 = 0.81$; RCP8.5, $R^2 = 0.76$; Full, $R^2 = 0.78$. Uncertainty is indicated by the spread of grey points, which show the regression coefficients calculated using each individual ensemble member.

doing so, help us to understand the process at play. To do this, we construct a timeseries of ice production using the regression coefficients calculated from internal variability in a) 20th Century data only; b) RCP8.5 data only and c) the full timeseries, combined with timeseries of the regressor climate variables from the ensemble mean. All three solutions for sea ice production successfully reconstruct the overall shape and interannual variability in the ensemble mean over the full period. The linear model also accurately captures the timing of the turning point from rising to falling ice production.

In light of the success of the linear model at reconstructing forced changes in sea ice production, we can next interrogate the contributions made by the different explanatory variables (Fig. 6b). Interpretation of these trends should critically consider that each regressor, except for Sep 10 m T, contains the product of surface air temperatures (as ΔT) and another climate variable. The trends of the underlying timeseries (Fig. 7) provide useful context.

The greatest contribution to increasing ice production up to 2020 comes from the $\beta_2 \Delta T A_{Sep}$ term. This term can be interpreted as ice produced in the open water available at the start of the freezing season. As the September open water area increases during 1970–2020 (Figs. 2a & 7b), this term contributes increasing ice production, despite SAT warming. As the ensemble mean Sep sea ice area approaches zero at around 2020 (Fig. 7b), this negative feedback on sea ice loss approaches

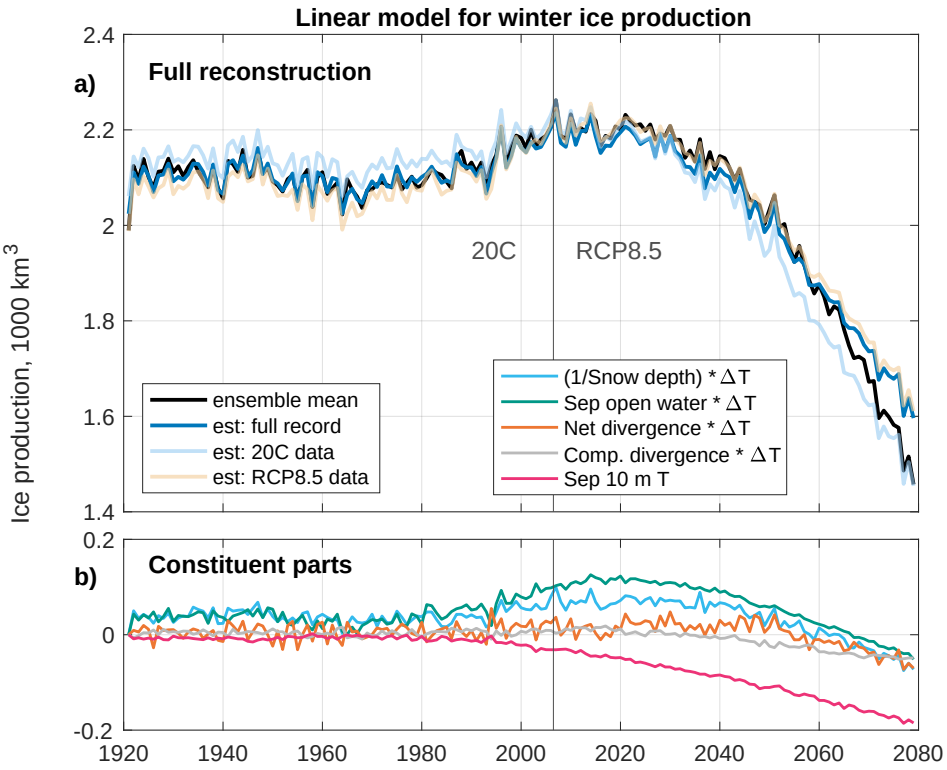

Figure 6. a) Ensemble mean winter sea ice production (black line), and reconstruction of ensemble mean using regressions trained on internal variability over the 20th Century run (light blue line), RCP8.5 run (light orange line) and full 1920–2080 timeseries (heavy blue line). b) Contribution to the reconstruction made by each component of the linear model, when trained upon internal variability from the full timeseries, plotted relative to the first winter (1920/1921).

a limit. From this point, A_{Sep} is fixed, while ΔT continues to fall (as SAT rises), resulting in a negative trend in the ice production attributable to the September open water setting.

Decreasing snow thickness on sea ice also provides an important contribution to rising ice production between c. 1980–2010 (Fig. 6b). While snow continues to thin to 2080 (Fig. 7f), after c. 2030 this thinning is out-competed by the effect of warming SAT, and the $\beta_1 \Delta T / h_s$ term contributes to a decline in ice production.

The two terms associated with divergence show more muted forced changes, owing to a close balance through time between the positive effects of divergence and the negative effects of SAT on ice production. However, in both terms, warming air temperatures begin to out-compete increasing divergence from the mid-21st century onwards. The $\beta_3 \Delta T A_{net}$ term also clearly contributes to ensemble mean interannual variability in ice production, reinforcing the important role of variability in wind-driven sea ice divergence in explaining year-to-year changes in ice production in the Kara-Laptev region.[35]

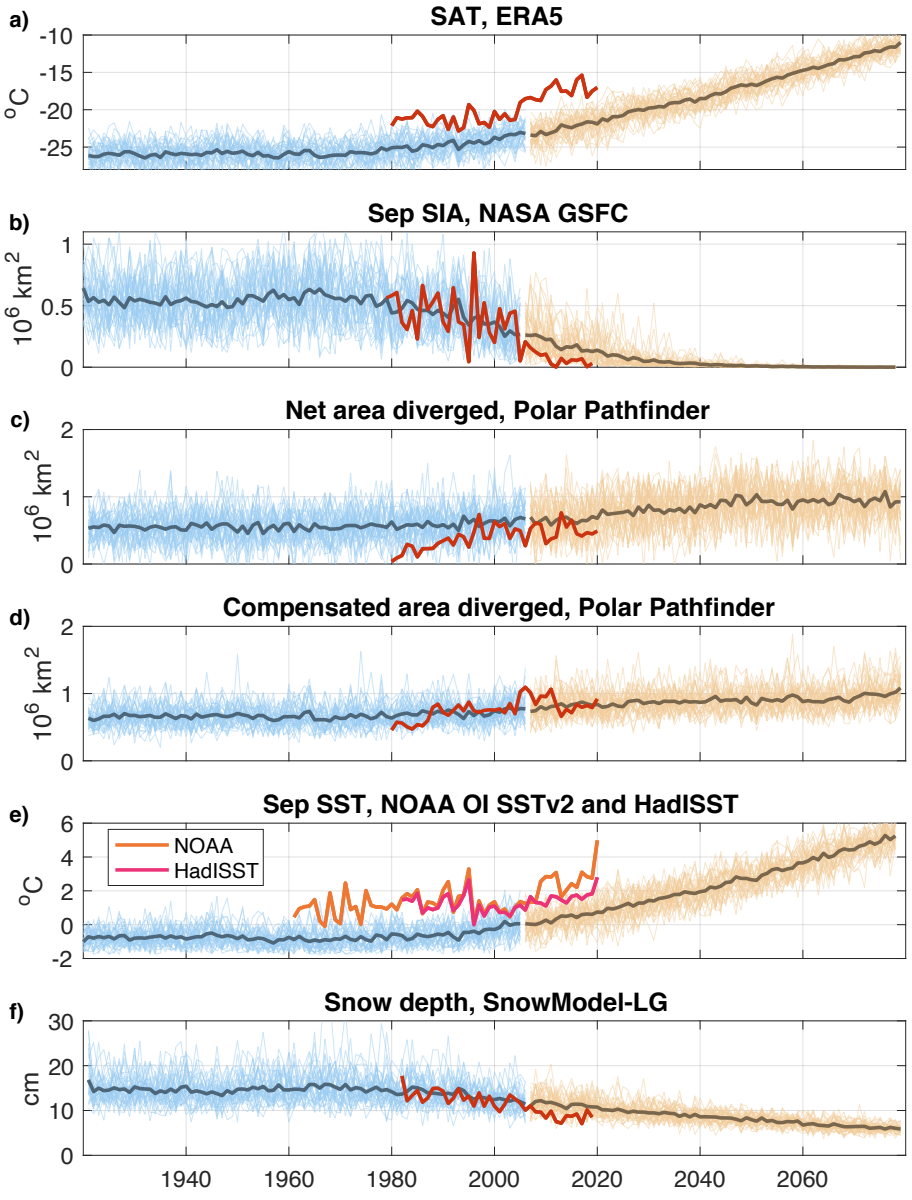

Figure 7. Timeseries of linear model inputs from CESM-LE, with real-world estimates superimposed in red: a) surface air temperatures, b) September sea ice area, c) net area diverged, d) compensated area diverged, e) September 10 m T in CESM-LE and SST in NOAA OI SSTv2, f) snow depth on ice. The 20th Century run is shown in blue and the RCP8.5 run in orange; ensemble mean indicated by darker line.

The $\beta_5 \mathrm{SST}_{Sep}$ term, though showing the weakest regression coefficient in the internal variability space, is the dominant driver of the forced decline in ice production. Indeed, Sep 10 m temperature exhibits a clear warming trend in the RCP8.5 run that rapidly departs from the range of 20th Century internal variability (Fig. 7e). There is evidently, then, a strong role for ocean heat derived from summer heating in delaying the freezing season and thus decreasing ice production. But is there a role for ocean heat in changing growth rate or ice production once the freezing season has begun? Ocean-to-ice heat fluxes (F_w) in the region are generally low during 20C at c. 0.5 W/m^2, rising throughout RCP8.5 to nearly 2 W/m^2 by 2080. This, however, does not appear to noticeably impede ice growth in CESM-LE: F_w is a statistically insignificant term when included in linear models for both ice production and growth rate, even in RCP8.5 (not shown).

Application to the observed Arctic

We next attempt to reconstruct changes in the Kara-Laptev region by applying observation-based estimates of the relevant climate variables to our linear model for ice production (Fig. 8). We use the regression coefficients derived from internal variability over the full run of CESM-LE. Note that this reconstruction using historical climate data is more analogous to the ice production in a single ensemble member of CESM-LE, rather than the (smooth) ensemble mean. The 10-year running mean in Fig. 8, however, exhibits a strikingly similarity to the ensemble mean trend in CESM-LE: reconstructed winter ice production increases by 150-200 km^3 from 1983 to 2000. From about the mid-2000s, ice production appears to show a slight decline. While uncertainty is difficult to constrain from the underlying observation-based estimates, we note that the reconstruction is somewhat sensitive to the choice of product for SST, especially from 2006/2007 onwards.

Unlike in CESM-LE, the $\beta_2 \Delta T A_{Sep}$ term is not the dominant driver of the reconstructed increase in ice production. We can reconcile this by noticing the anticorrelation ($R = -0.77$) between the Sep SIA and SAT timeseries (Fig. 7a,b). Both timeseries show marked jumps in the winter 2005/2006—these changes act in opposing directions in terms of ice production and thus tend to cancel one another out. Given that the September open water area has already reached a maximum (as September SIA has declined to zero in recent years), we can expect future atmospheric warming to yield a negative ice production trend from this term, as per Fig. 6b.

Examining the trends from the other terms, we see that September SSTs exert a negative influence on ice production from the 2000s. The inverse snow thickness term $\beta_1 \Delta T / h_s$ causes marked interannual variability and a strong positive trend in ice production: snow thinning out-competes warming over this period.

The contributions to ice production from the two divergent settings exhibit perhaps the strongest rises in the mid-part of the timeseries, out-competing atmospheric warming, until plateauing or shallowly declining in the final c. 15 years.

Discussion

Although CESM-LE is a complex coupled climate model, we have shown that we can understand variability and trends in ice production in the Arctic Ocean's "ice factories" using a simple equation. Our analysis shows that a number of negative feedback to ice loss—increasing September open water, increasing divergence, reducing snow depth—contribute to a gradual

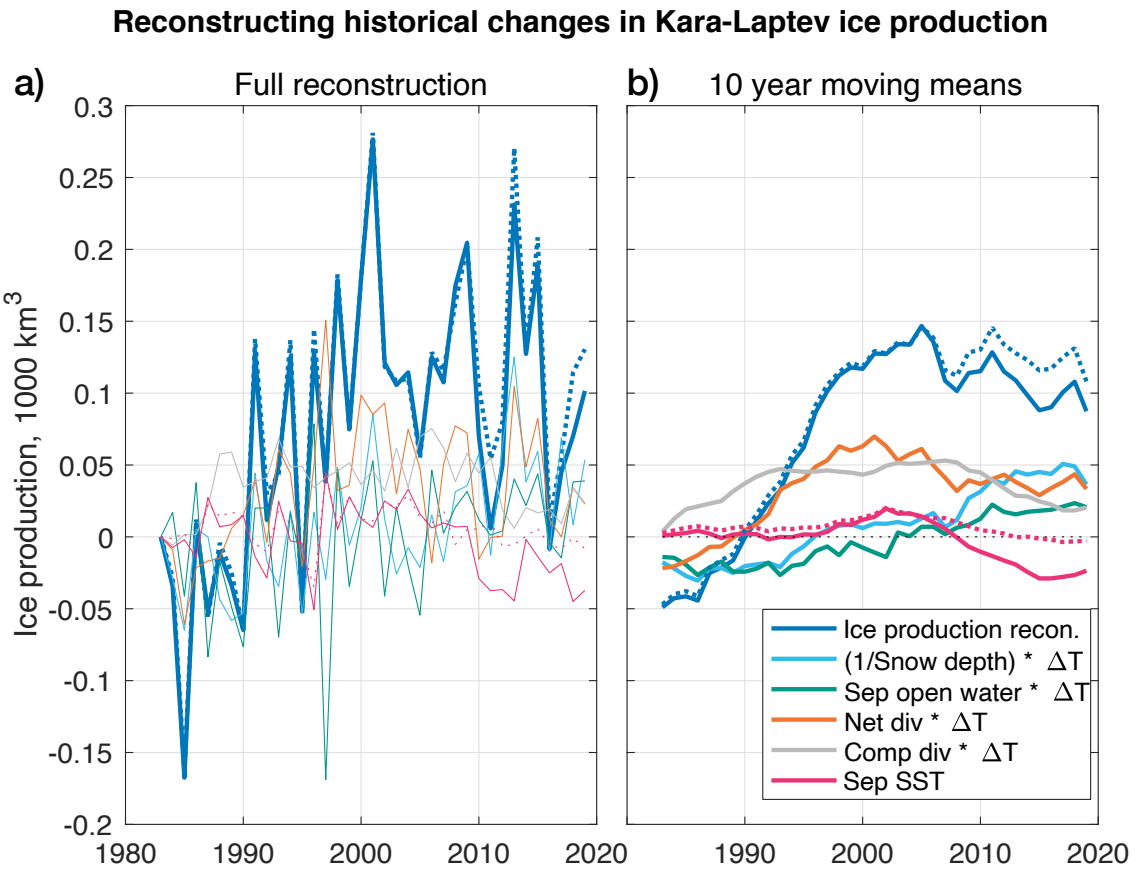

Figure 8. Reconstruction of historical changes in the winter ice production in the Kara and Laptev seas relative to the first winter of the reconstruction (1982/1983). Reconstruction uses climate variables from observation-based estimates and the linear model trained on CESM-LE internal variability. Data are plotted with respect to the new year of the winter in question. Dashed line is the result of using NOAA OI V2 SST product, while the solid line uses HadISST.

rise in ice production in CESM-LE from c. 1970–2010, but are increasingly outcompeted by atmospheric warming through the 21st Century under the RCP8.5 emissions pathway. Together with an important contribution from increasing upper ocean temperatures at the end of summer, this leads to a decline in ice production.

In CESM-LE, the timing of peak ice production is primarily set by the timing at which September sea ice area in the Kara-Laptev region approaches zero. At this point, one of the leading negative feedbacks to the loss of ice—the expansion of the September open water area—has reached a limit and can no longer contribute additional ice production. Continued atmospheric warming then ensures a decrease in the ice production attributed to this setting. In observational data, we see that the expansion of the September open water area has also reached a limit in recent years. As such, we should expect ice production in the Kara and Laptev seas to decline in the coming decades under continued greenhouse forcing.

In our reconstruction of historical changes in Kara-Laptev sea ice production, using observation-based estimates of the relevant climate variables, we see a similar trend to that shown by CESM-LE over the same time window. Reconstructed ice production appears to be currently passing a peak, with the recent warm winters of 2015/2016 and 2016/2017[28,29,19] notably triggering relatively low ice production.

Sea ice from the Kara and Laptev seas carries sediment, pollutants, trace elements and gases into the central Arctic and beyond.[54,35,55] Falling sea ice production in the region will therefore affect redistribution of biogeochemical matter in the Arctic Ocean, with implications for primary production and biodiversity.[54]

As the sea ice production in the Kara and Laptev seas begins to fall, we might question how other areas of the Arctic Ocean will fare. While much of the process-based understanding we have developed for the Kara-Laptev region is transferable to other areas, there are important differences in the mean sea ice state and oceanic setting that affect the balance of F_c and F_w. As ice is generally thin in the Kara and Laptev seas, owing to the wind-driven time-mean divergence of sea ice, and because little ice survives the summer, F_c is comparatively large (Equation 2). On the other hand, once the excess heat stored in the upper ocean has been removed to the atmosphere, F_w is small. In other regions this balance may differ.

The same processes identified in our linear model that drive increasing ice production (by increasing F_c) in the Kara-Laptev region during 1970–2010 are likely to become increasingly important in the central Arctic. As the September sea ice edge progressively retreats through the central Arctic (Fig. 2a), we can expect year-on-year increases in Sep open water area and sea ice divergence, and decreases in snow depth in these regions—all of which drive increasing ice production and are negative feedbacks on sea ice loss. In CESM-LE, the share of Kara-Laptev ice production in the Arctic Ocean (excluding Barents Sea) declines from 25% in the 20th Century run to 19% by 2080 (it comprises 16% of the area).

These shifting patterns of ice production raise important questions for the stability of the Arctic halocline. High rates of freezing in the Kara and Laptev seas strengthen the cold halocline of the central Arctic basins, which limits upwards heat fluxes from Atlantic Waters and restricts the depth of water that is convectively cooled prior to and during sea ice growth.[56] Freezing in the Kara and Laptev seas can stabilise the halocline via the advective interleaving of cold shelf waters, densified by brine rejection, into the halocline of the Eurasian Basin.[43,57] Another mechanism is that winter convection down to the halocline is followed by surface injection of cold and fresh waters (from the melting of shelf-derived sea ice), thus renewing the cold halocline via a 'convective mode'.[44,58] Both mechanisms may operate in different seasonal and spatial contexts,[59,60,37] and both depend on ice production on the shelves. Meanwhile, increasing ice production and brine rejection in the Eurasian basin interior may weaken the halocline by encouraging vigorous convection, allowing heat from the Atlantic Waters to reach the surface.[48,46]

In waters deeper than the shelfbreak, we expect a more important role for F_w in determining ice production on account of the availability of deep Atlantic heat. In the future, ocean-to-ice heat fluxes are likely to play a greater role in limiting sea ice production in the Arctic, a trend that may have already begun.[61] In the shallow waters of the Kara and Laptev polynyas, on the other hand, winter convection may propagate to the seafloor,[32,39] but because Atlantic Waters rarely upwell into these shallow areas where freezing is most intense, increases in F_w from such mixing should be limited, though Atlantic Waters may warm halocline waters that intrude onto the shelf.[62] Nonetheless, in our linear model for sea ice production, F_w is an insignificant

term even in the RCP8.5 run up to 2080. However, in other areas of the Arctic, and indeed the Antarctic, F_w is likely to be important.

Our reconstruction of forced changes in sea ice production in the Kara-Laptev region (Fig. 6) shows that it is the heat stored in the upper ocean at the end of summer, rather than heat fluxed from below during the freezing season, that is more important in restricting ice production. A greater reservoir of summer heat requires more time to cool, thus shortening the freezing season (reducing the *usage* of the ice factory). September upper ocean temperatures can be expected to continue to rise as a result of increasing solar radiation (due to reducing summer sea ice concentration), increasing radiative forcing, and increasing (and warming) river runoff.[63,64]

In this paper we developed a simple linear model that captures ice production in key "ice factories" of the Arctic Ocean. Ice production in these regions is most likely presently passing a peak, and will soon begin a long-term decline if greenhouse gas concentrations continue to rise. Reduced ice production in the Kara and Laptev seas will alter the physical and biological makeup of the Arctic Ocean, and we suggest that future work should address the profound impact of these forseeable changes.

Methods

Climate model

To analyse the forced response of sea ice production in the Kara and Laptev seas to climate change, we use data from 35 of the 40 ensemble members of the Community Earth System Model Large Ensemble (CESM-LE).[65] A large ensemble such as CESM-LE permits investigation of forced responses to climate change in the context of internal climate variability.[65] CESM-LE is based on the fully coupled model CESM1.1, and comprises the Community Atmosphere Model, version 5 (CAM5); the Parallel Ocean Program, version 2 (POP2); the Community Land Model, version 4; and the Los Alamos Sea Ice Model CICE, version 4 as its sea ice component. The version of CICE used features improvements to shortwave radiation interactions, including the effects of melt ponds and aerosol deposition on ice.[66] The spatial resolution of the CESM1.1 ocean and sea ice models is nominally $1^\circ \times 1^\circ$ longitude by latitude, while the atmospheric model is $0.9^\circ \times 1.25^\circ$.

All CESM-LE ensemble members are forced by the same external forcing data, separated into two runs. Firstly, a run from 1920–2005 forced by historical external forcing data[67] that we refer to as the 20th Century run; secondly, from 2006–2100, a high-emissions RCP8.5 run,[68] leading to over 4 °C warming by 2100. The RCP8.5 pathway at present slightly underestimates observed emissions; it presently represents a realistic or even conservative scenario.[69,70] Additionally, it provides big signal, which helps us to interpret climate dynamics in the presence of noise. The ensemble spread is entirely generated by simulated internal climate variability originating from very small, random differences in the initial air temperature fields.

Here we rely on monthly data between 1920–2080—sufficient time to assess major forced changes in ice production in the Kara and Laptev seas—from 35 ensemble members. Previous Arctic studies have investigated the impact of subsampling the ensemble.[71,72,73] The number of ensemble members required varies according to the nature of the climate variables under investigation. For coarse metrics such as winter means, we are confident that 35 ensemble members is sufficient.

CESM1.1 and CESM-LE have been used in a broad swathe of Arctic climate studies and generally perform well.[74,71,75,76,77,73,78,79,31] Arctic sea ice thickness in CESM-LE broadly corresponds in spatial mean pattern and trend during 1980–2015 with PIOMAS,[80] though exhibits slightly thicker (order several 10 cm) sea ice than PIOMAS.[81,31] Although the satellite record of sea ice thickness is short, CESM-LE compares well with estimates of inter-seasonal thickness changes and interannual variability.[31] Declining Arctic sea ice concentration and extent in CESM-LE has been more comprehensively compared to observations, which fit within its ensemble spread and compare well across all seasons.[77,71,73] The changing open water season also shows correspondence with satellite observations, including in the Laptev Sea.[73]

Climate variables computed

To capture winter thermodynamic sea ice production, we use monthly data from October to April, inclusive, as per Petty et al.[31] In contrast with Petty et al., we analyse freshwater exchanges with the ocean, rather than changes in ice thickness, to explicitly isolate thermodynamic changes. Sea ice production is calculated as the sum of only the ocean-to-ice part of thermodynamic ice-ocean freshwater fluxes.

Our calculation of freezing area days using CESM-LE data is an approximation, dependent on the spatial discretisation of the ocean and sea ice components (nominally $1^\circ \times 1^\circ$), temporal averaging (monthly) and number of ensemble members used (35). The mean winter growth rate in all such freezing grid cells is given by the total winter ice production divided by the number of freezing area days.

The other variables we consider here are: snow depth on sea ice (note that this is different to snow volume per unit grid cell area), sea ice concentration, sea ice divergence, surface air temperatures, and ocean temperatures in the top (10 m thick) grid cell. We investigate two types of sea ice divergence. Firstly, the *net* divergence, which—by the divergence theorem—is equivalent to the area expansion of the sea ice area, or, when that area encompasses the whole Kara-Laptev region, it is the area export of sea ice from the region. We are also interested in divergence within the region that is compensated by convergence somewhere else in the region; this divergence can open or expand leads but still not lead to export. To capture this compensated divergence, we record the *positive* divergence, which is counted only over cells where the divergence is positive. The compensated divergence is then found as $compensated\ div = positive\ div - net\ div$.

All parameters are computed over the study region shown in Figure 1 and appropriately area-weighted. The Kara-Laptev region is defined by the coastline and the following (lat,lon) vertices: (72.5,70), (82,70), (82,110), (78,110), (78,150), (72,150).

When plotting data, we identify the winter spanning years n and $n+1$ with year $n+1$; the winter 2015/2016 is labelled 2016. The variables extracted from the observation-derived estimates are computed in a consistent manner to their equivalents from CESM-LE.

Observation-based estimates

We use monthly mean 2 m temperatures from the ERA5 global reanalysis,[82] gridded at $0.25^\circ \times 0.25^\circ$ resolution. ERA5 is the fifth generation of atmospheric reanalyses from the European Centre for Medium-Term Weather Forecasting (ECMWF). We use the terms surface air temperature and 2 m temperature interchangeably here. Surface air temperatures from ERA5 generally

perform well in the Arctic relative to in situ observations, however consistently show warm biases of order several degrees over sea ice in winter months.[83]Our analysis of these data spans the winters 1979/1980 to 2019/2020.

To plot mean sea ice velocities and calculate sea ice divergence, we make use of the National Snow and Ice Data Center (NSIDC) Polar Pathfinder v4.1 product, gridded at 25×25 km resolution and in weekly means.[49] We analyse data from Polar Pathfinder encompassing the winters 1979/1980 to 2019/2020.

To document changes in sea ice area, we use sea ice concentration data from passive microwave satellite retrievals, prepared by the NASA Goddard Space Flight Centre (NASA GSFC). We use the 'merged' data, which combines data derived from the Bootstrap and Nasa Team algorithms,[84] and compares well with other estimates.[85,86] We use data spanning the winters 1978/1979 to 2018/2019.

For snow depth, we use data from a Lagrangian snow evolution model, SnowModel-LG, which provides daily data on a 25 km × 25 km grid and is forced by the MERRA-2 atmospheric reanalysis.[87] SnowModel-LG compares well to observational datasets in spatial and seasonal variability of snow depth and density.[88] The dataset spans winters 1981/1982 to 2018/2019. Consistent with our snow depth acquisitions from CESM-LE, we present snow thickness on sea ice where present.

For sea surface temperatures, we use the Met Office Hadley Centre's sea ice and sea surface temperature (SST) data set, HadISST1.[89] The monthly data are provided on a 1°×1° grid. We use data spanning the winters 1961/1962 to 2019/2020. The SST data are taken from the Met Office Marine Data Bank (MDB), as well as data from the Comprehensive Ocean-Atmosphere Data Set (COADS) (now ICOADS) where there were no MDB data. The sea ice data are taken from a variety of sources including passive microwave retrievals and digitized sea ice charts. Additionally, we use monthly-mean SST data at a 1°×1° resolution from the National Oceanic and Atmospheric Administration Optimum Interpolation Sea Surface Temperature v2 (NOAA OISSTv2) dataset.[90] We use NOAA OISSTv2 data from the winters 1981/1982 to 2019/2020.

Data availability

CESM-LE data are accessible at the NCAR/UCAR CESM website: https://www.cesm.ucar.edu/projects/community-projects/LENS/data-sets.html.

ERA5 data are accessible via the Copernicus Climate Change Service portal (https://cds.climate.copernicus.eu/).

Polar Pathfinder sea ice motion data are accessible at the NSIDC website (https://doi.org/10.5067/INAWUWO7QH7B).

The NASA GSFC sea ice concentration data are accessible at the NSIDC website (https://doi.org/10.7265/N59P2ZTG).

SnowModel-LG data are available at the NSIDC website (Liston, G. E., J. Stroeve, and P. Itkin; Lagrangian Snow Distributions for Sea-Ice Applications; http://dx.doi.org/10.5067/27A0P5M6LZBI).

HadISST data were obtained from https://www.metoffice.gov.uk/hadobs/hadisst/ and are © Crown Copyright, Met Office, 2003, provided under a Non-Commercial Government Licence http://www.nationalarchives.gov.uk/doc/non-commercial-government-licence/version/2/

The NOAA OISSTv2 dataset is provided by the NOAA/OAR/ESRL PSL, Boulder, Colorado, USA, and accessible at their website (https://psl.noaa.gov/data/gridded/data.noaa.oisst.v2.html).

Code availability. Code is available from the corresponding author upon request.

Author contributions. S.C. formulated the study with input from H.J and Y.K.. A.R acquired the CESM-LE data. S.C. carried out the main analysis with CESM-LE and the observation-based products, R.M. contributed analysis of SnowModel-LG and J.D. contributed additional CESM-LE analysis. All authors contributed to the development of the study. S.C led the writing with significant input from all authors.

Competing interests. The authors declare no competing interests.

Acknowledgements. SC and AR were both supported by DTP studentships under UK NERC grant NE/L002612/1. RM was also supported via a UK NERC DTP grant (NE/L002485/1). HJ acknowledges support from the UK NERC under ArctiCONNECT (NE/V005855/1). JD was supported by the Research Council of Norway project Nansen Legacy (grant 276730). YK acknowledges funding from TICTOC grant NE/P019064/1.

References

[1] Notz, D. & Stroeve, J. C. Observed Arctic sea-ice loss directly follows anthropogenic CO2 emission. *Science* **354**, 747–750 (2016).

[2] Manabe, S. & Stouffer, R. J. Sensitivity of a global climate model to an increase of CO2 concentration in the atmosphere. *Journal of Geophysical Research* **85**, 5529–5554 (1980).

[3] Serreze, M. C., Barrett, A. P., Stroeve, J. C., Kindig, D. N. & Holland, M. M. The emergence of surface-based Arctic amplification. *Cryosphere* **3**, 11–19 (2009).

[4] Goosse, H. *et al.* Quantifying climate feedbacks in polar regions. *Nature Communications* **9** (2018). http://dx.doi.org/10.1038/s41467-018-04173-0.

[5] Stroeve, J. C. & Notz, D. Changing state of Arctic sea ice across all seasons. *Environmental Research Letters* **13** (2018).

[6] Kwok, R. Arctic sea ice thickness, volume, and multiyear ice coverage: Losses and coupled variability (1958-2018). *Environmental Research Letters* **13** (2018).

[7] Martin, T., Tsamados, M., Schroeder, D. & Feltham, D. L. The impact of variable sea ice roughness on changes in Arctic Ocean surface stress: A model study. *Journal of Geophysical Research: Oceans* **121**, 1931–1952 (2016). https://onlinelibrary.wiley.com/doi/abs/10.1002/2015JC011186.

[8] Aagaard, K. & Carmack, E. C. The role of sea ice and other fresh water in the Arctic circulation. *Journal of Geophysical Research* **94**, 14485–14498 (1989).

[9] Steele, M. & Flato, G. M. Sea Ice Growth , Melt , and Modeling : A Survey. In NATO & ARW (eds.) *The Arctic Ocean Freshwater Budget*, January (2000).

[10] Serreze, M. C. & Barry, R. G. Processes and impacts of Arctic amplification: A research synthesis. *Global and Planetary Change* **77**, 85–96 (2011). http://dx.doi.org/10.1016/j.gloplacha.2011.03.004.

[11] Haine, T. W. & Martin, T. The Arctic-Subarctic sea ice system is entering a seasonal regime: Implications for future Arctic amplification. *Scientific Reports* **7**, 1–9 (2017).

[12] Maykut, G. A. Energy exchange over young sea ice in the central Arctic. *Journal of Geophysical Research* **83**, 3646 (1978).

[13] Lang, A., Yang, S. & Kaas, E. Sea ice thickness and recent Arctic warming. *Geophysical Research Letters* **44**, 409–418 (2017).

[14] Tietsche, S., Notz, D., Jungclaus, J. H. & Marotzke, J. Recovery mechanisms of Arctic summer sea ice. *Geophysical Research Letters* **38**, 1–4 (2011).

[15] Bintanja, R., Graversen, R. G. & Hazeleger, W. Arctic winter warming amplified by the thermal inversion and consequent low infrared cooling to space. *Nature Geoscience* **4**, 758–761 (2011).

[16] Payne, A. E., Jansen, M. F. & Cronin, T. W. Conceptual model analysis of the influence of temperature feedbacks on polar amplification. *Geophysical Research Letters* **42**, 9561–9570 (2015).

[17] Pithan, F. & Mauritsen, T. Arctic amplification dominated by temperature feedbacks in contemporary climate models. *Nature Geoscience* **7**, 181–184 (2014).

[18] Bitz, C. M. & Roe, G. H. A mechanism for the high rate of sea ice thinning in the Arctic Ocean. *Journal of Climate* **17**, 3623–3632 (2004).

[19] Stroeve, J. C., Schroder, D., Tsamados, M. & Feltham, D. Warm winter, thin ice? *Cryosphere* **12**, 1791–1809 (2018).

[20] Merkouriadi, I., Cheng, B., Graham, R. M., Rösel, A. & Granskog, M. A. Critical Role of Snow on Sea Ice Growth in the Atlantic Sector of the Arctic Ocean. *Geophysical Research Letters* **44**, 479–10 (2017).

[21] Notz, D. The future of ice sheets and sea ice: Between reversible retreat and unstoppable loss. *Proceedings of the National Academy of Sciences of the United States of America* **106**, 20590–20595 (2009).

[22] Bigdeli, A., Nguyen, A. T., Pillar, H. R., Ocaña, V. & Heimbach, P. Atmospheric Warming Drives Growth in Arctic Sea Ice: A Key Role for Snow. *Geophysical Research Letters* **47**, 1–10 (2020).

[23] Rampal, P., Weiss, J. & Marsan, D. Positive trend in the mean speed and deformation rate of Arctic sea ice, 1979-2007. *Journal of Geophysical Research: Oceans* **114**, 1–14 (2009).

[24] Kwok, R., Spreen, G. & Pang, S. Arctic sea ice circulation and drift speed: Decadal trends and ocean currents. *Journal of Geophysical Research: Oceans* **118**, 2408–2425 (2013).

[25] Spreen, G., Kwok, R. & Menemenlis, D. Trends in Arctic sea ice drift and role of wind forcing: 1992-2009. *Geophysical Research Letters* **38** (2011).

[26] Hibler, W. D. A Dynamic Thermodynamic Sea Ice Model. *Journal of Physical Oceanography* **9**, 815–846 (1979). http://library1.nida.ac.th/termpaper6/sd/2554/19755.pdfhttp://journals.ametsoc.org/doi/10.1175/1520-0485(1979)009%3C0815:ADTSIM%3E2.0.CO;2.

[27] Eisenman, I. & Wettlaufer, J. S. Nonlinear threshold behavior during the loss of Arctic sea ice. *Proceedings of the National Academy of Sciences of the United States of America* **106**, 28–32 (2009).

[28] Boisvert, L. N., Petty, A. A. & Stroeve, J. C. The impact of the extreme winter 2015/16 arctic cyclone on the Barents-Kara Seas. *Monthly Weather Review* **144**, 4279–4287 (2016).

[29] Ricker, R. *et al.* Satellite-observed drop of Arctic sea ice growth in winter 2015–2016. *Geophysical Research Letters* **44**, 3236–3245 (2017).

[30] Graham, R. M. *et al.* Increasing frequency and duration of Arctic winter warming events. *Geophysical Research Letters* **44**, 6974–6983 (2017).

[31] Petty, A. A., Holland, M. M., Bailey, D. A. & Kurtz, N. T. Warm Arctic, Increased Winter Sea Ice Growth? *Geophysical Research Letters* **45**, 922–12 (2018).

[32] Reimnitz, E., Dethleff, D. & Nürnberg, D. Contrasts in Arctic shelf sea-ice regimes and some implications: Beaufort Sea versus Laptev Sea. *Marine Geology* **119**, 215–225 (1994).

[33] Carmack, E. C. & Wassmann, P. Food webs and physical-biological coupling on pan-Arctic shelves: Unifying concepts and comprehensive perspectives. *Progress in Oceanography* **71**, 446–477 (2006).

[34] Gordeev, V. V., Martin, J. M., Sidorov, I. S. & Sidorova, M. V. A reassessment of the Eurasian river input of water, sediment, major elements, and nutrients to the Arctic Ocean. *American Journal of Science* **296**, 664–691 (1996). http://www.ajsonline.org/cgi/doi/10.2475/ajs.296.6.664.

[35] Rigor, I. G. & Colony, R. Sea-ice production and transport of pollutants in the Laptev Sea, 1979- 1993. *Science of the Total Environment* **202**, 89–110 (1997).

[36] Alexandrov, V. Y. *et al.* Sea ice circulation in the Laptev Sea and ice export to the Arctic Ocean: Results from satellite remote sensing and numerical modeling. *Journal of Geophysical Research: Oceans* **105**, 17143–17159 (2000). http://doi.wiley.com/10.1029/2000JC900029.

[37] Pemberton, P., Nilsson, J. & Meier, H. E. Arctic ocean freshwater composition, pathways and transformations from a passive tracer simulation. *Tellus, Series A: Dynamic Meteorology and Oceanography* **66** (2014).

[38] Tamura, T. & Ohshima, K. I. Mapping of sea ice production in the Arctic coastal polynyas. *Journal of Geophysical Research: Oceans* **116**, 1–20 (2011).

[39] Dmitrenko, I. A. *et al.* Impact of flaw polynyas on the hydrography of the Laptev Sea. *Global and Planetary Change* **48**, 9–27 (2005).

[40] Martin, S. & Cavalieri, D. J. Contributions of the siberian shelf polynyas to the arctic ocean intermediate and deep water. *Journal of Geophysical Research: Oceans* **94**, 725–738 (1989).

[41] Armitage, T. W., Bacon, S. & Kwok, R. Arctic Sea Level and Surface Circulation Response to the Arctic Oscillation. *Geophysical Research Letters* **45**, 6576–6584 (2018).

[42] Rigor, I. G., Wallace, J. M. & Colony, R. L. Response of sea ice to the Arctic Oscillation. *Journal of Climate* **15**, 2648–2663 (2002). http://iapb.apl.washington.edu.

[43] Aagaard, K., Coachman, L. K. & Carmack, E. C. On the halocline of the Arctic Ocean. *Deep Sea Research Part A, Oceanographic Research Papers* **28**, 529–545 (1981).

[44] Rudels, B., Jones, E. P., Anderson, L. G. & Kattner, G. On the Intermediate Depth Waters of the Arctic Ocean. In Johannessen, O., Muench, R. & Overland, J. (eds.) *The Polar Oceans and Their Role in Shaping the Global Environment: The Nansen Centennial Volume, Geophysical Monograph Series, vol. 85*, 33–46 (AGU, Washington, D.C., 1994). http://doi.wiley.com/10.1029/GM085p0033.

[45] Polyakov, I. V., Pnyushkov, A. V. & Carmack, E. C. Stability of the arctic halocline: A new indicator of arctic climate change. *Environmental Research Letters* **13** (2018).

[46] Polyakov, I. V. *et al.* Greater role for Atlantic inflows on sea-ice loss in the Eurasian Basin of the Arctic Ocean. *Science* **356**, 285–291 (2017).

[47] Lind, S., Ingvaldsen, R. B. & Furevik, T. Arctic warming hotspot in the northern Barents Sea linked to declining sea-ice import. *Nature Climate Change* **8**, 634–639 (2018).

[48] Polyakov, I. V. *et al.* Weakening of cold halocline layer exposes sea ice to oceanic heat in the eastern arctic ocean. *Journal of Climate* **33**, 8107–8123 (2020).

[49] Tschudi, M. A., Meier, W. N., Stewart, J., Fowler, C. & Maslanik, J. A. Polar Pathfinder Daily 25 km EASE-Grid Sea Ice Motion Vectors, Version 4. [1978-2018] (2019). https://nsidc.org/data/nsidc-0116/versions/4.

[50] Stroeve, J. C. *et al.* The Arctic's rapidly shrinking sea ice cover: A research synthesis. *Climatic Change* **110**, 1005–1027 (2012).

[51] Petrich, C. & Eicken, H. Growth, Structure and Properties of Sea Ice. In Thomas, D. N. & Dieckmann, G. S. (eds.) *Sea Ice*, chap. 2, 79–113 (Wiley-Blackwell, 2010).

[52] Carmack, E. C. *et al.* Toward quantifying the increasing role of oceanic heat in sea ice loss in the new arctic. *Bulletin of the American Meteorological Society* **96**, 2079–2105 (2015).

[53] Wadhams, P. Sea ice thickness distribution in Fram Strait. *Nature* **305**, 108–111 (1983).

[54] Krumpen, T. *et al.* Arctic warming interrupts the Transpolar Drift and affects long-range transport of sea ice and ice-rafted matter. *Scientific Reports* **9**, 1–9 (2019).

[55] Peeken, I. *et al.* Arctic sea ice is an important temporal sink and means of transport for microplastic. *Nature Communications* **9**, 1505 (2018). http://dx.doi.org/10.1038/s41467-018-03825-5http://www.nature.com/articles/s41467-018-03825-5.

[56] Bulgakov, N. P. The role of convection in the mechanism of heat transfer of deep Atlantic water. *Deep-Sea Research and Oceanographic Abstracts* **9**, 233–239 (1962).

[57] Jones, E. P. & Anderson, L. G. On the origin of the chemical properties of the Arctic Ocean halocline. *Journal of Geophysical Research* **91**, 10759 (1986). http://doi.wiley.com/10.1029/JC091iC09p10759.

[58] Rudels, B., Jones, E. P., Schauer, U. & Eriksson, P. Atlantic sources of the Arctic Ocean surface and halocline waters. *Polar Research* **23**, 181–208 (2004). http://www.polarresearch.net/index.php/polar/article/view/6278.

[59] Steele, M. & Boyd, T. Retreat of the cold halocline layer in the Arctic Ocean. *Journal of Geophysical Research: Oceans* **103**, 10419–10435 (1998). http://doi.wiley.com/10.1029/98JC00580.

[60] Woodgate, R. A. *et al.* The Arctic Ocean boundary current along the Eurasian slope and the adjacent Lomonosov ridge: Water mass properties, transports and transformations from moored instruments. *Deep-Sea Research Part I: Oceanographic Research Papers* **48**, 1757–1792 (2001).

[61] Ricker, R. *et al.* Evidence for an increasing role of ocean heat in arctic winter sea ice growth. *Journal of Climate* **34**, 5215–5227 (2021).

[62] Dmitrenko, I. A. *et al.* Impact of the Arctic Ocean Atlantic water layer on Siberian shelf hydrography. *Journal of Geophysical Research: Oceans* **115**, 1–17 (2010).

[63] Whitefield, J., Winsor, P., McClelland, J. & Menemenlis, D. A new river discharge and river temperature climatology data set for the pan-Arctic region. *Ocean Modelling* **88**, 1–15 (2015). https://linkinghub.elsevier.com/retrieve/pii/S1463500315000025.

[64] Zanowski, H., Jahn, A. & Holland, M. M. Arctic Ocean freshwater in CMIP6 Ensembles: Declining Sea Ice, Increasing Ocean Storage and Export. *Journal of Geophysical Research: Oceans* (2021). https://onlinelibrary.wiley.com/doi/10.1029/2020JC016930.

[65] Kay, J. E. *et al.* The community earth system model (CESM) large ensemble project : A community resource for studying climate change in the presence of internal climate variability. *Bulletin of the American Meteorological Society* **96**, 1333–1349 (2015).

[66] Holland, M. M., Bailey, D. A., Briegleb, B. P., Light, B. & Hunke, E. Improved Sea Ice Shortwave Radiation Physics in CCSM4: The Impact of Melt Ponds and Aerosols on Arctic Sea Ice. *Journal of Climate* **25**, 1413–1430 (2012). https://journals.ametsoc.org/doi/10.1175/JCLI-D-11-00078.1.

[67] Lamarque, J.-F. *et al.* Historical (1850–2000) gridded anthropogenic and biomass burning emissions of reactive gases and aerosols: methodology and application. *Atmospheric Chemistry and Physics* **10**, 7017–7039 (2010). https://acp.copernicus.org/articles/10/7017/2010/.

[68] Meinshausen, M. *et al.* The RCP greenhouse gas concentrations and their extensions from 1765 to 2300. *Climatic Change* **109**, 213–241 (2011). http://link.springer.com/10.1007/s10584-011-0156-z.

[69] Peters, G. P. *et al.* The challenge to keep global warming below 2C. *Nature Climate Change* **3**, 4–6 (2013).

[70] Schwalm, C. R., Glendon, S. & Duffy, P. B. RCP8.5 tracks cumulative CO2 emissions. *Proceedings of the National Academy of Sciences of the United States of America* **117**, 19656–19657 (2020).

[71] Jahn, A., Kay, J. E., Holland, M. M. & Hall, D. M. How predictable is the timing of a summer ice-free Arctic? *Geophysical Research Letters* **43**, 9113–9120 (2016).

[72] Jahn, A. & Laiho, R. Forced Changes in the Arctic Freshwater Budget Emerge in the Early 21st Century. *Geophysical Research Letters* **47**, 1–10 (2020).

[73] Barnhart, K. R., Miller, C. R., Overeem, I. & Kay, J. E. Mapping the future expansion of Arctic open water. *Nature Climate Change* **6**, 280–285 (2016).

[74] Årthun, M., Eldevik, T. & Smedsrud, L. H. The role of Atlantic heat transport in future Arctic winter sea ice loss. *Journal of Climate* **32**, 3327–3341 (2019).

[75] Jahn, A. Reduced probability of ice-free summers for 1.5 °C compared to 2 °C warming. *Nature Climate Change* **8**, 409–413 (2018). http://www.nature.com/articles/s41558-018-0127-8.

[76] Morrison, A. L., Kay, J. E., Frey, W. R., Chepfer, H. & Guzman, R. Cloud Response to Arctic Sea Ice Loss and Implications for Future Feedback in the CESM1 Climate Model. *Journal of Geophysical Research: Atmospheres* **124**, 1003–1020 (2019). https://onlinelibrary.wiley.com/doi/10.1029/2018JD029142.

[77] Swart, N. C., Fyfe, J. C., Hawkins, E., Kay, J. E. & Jahn, A. Influence of internal variability on Arctic sea-ice trends. *Nature Climate Change* **5**, 86–89 (2015).

[78] England, M., Jahn, A. & Polvani, L. Nonuniform Contribution of Internal Variability to Recent Arctic Sea Ice Loss. *Journal of Climate* **32**, 4039–4053 (2019). http://journals.ametsoc.org/doi/10.1175/JCLI-D-18-0864.1.

[79] DeRepentigny, P., Tremblay, L. B., Newton, R. & Pfirman, S. Patterns of Sea Ice Retreat in the Transition to a Seasonally Ice-Free Arctic. *Journal of Climate* **29**, 6993–7008 (2016). http://journals.ametsoc.org/doi/10.1175/JCLI-D-15-0733.1.

[80] Schweiger, A. *et al.* Uncertainty in modeled Arctic sea ice volume. *Journal of Geophysical Research: Oceans* **116**, 1–21 (2011).

[81] Labe, Z., Magnusdottir, G. & Stern, H. Variability of Arctic sea ice thickness using PIOMAS and the CESM large ensemble. *Journal of Climate* **31**, 3233–3247 (2018).

[82] Hersbach, H. *et al.* The ERA5 global reanalysis. *Quarterly Journal of the Royal Meteorological Society* **146**, 1999–2049 (2020).

[83] Wang, C., Graham, R. M., Wang, K., Gerland, S. & Granskog, M. A. Comparison of ERA5 and ERA-Interim near-surface air temperature, snowfall and precipitation over Arctic sea ice: effects on sea ice thermodynamics and evolution. *Cryosphere* **13**, 1661–1679 (2019).

[84] Comiso, J. C., Cavalieri, D. J., Parkinson, C. L. & Gloersen, P. Passive microwave algorithms for sea ice concentration: A comparison of two techniques. *Remote Sensing of Environment* **60**, 357–384 (1997). https://linkinghub.elsevier.com/retrieve/pii/S0034425796002209.

[85] Meier, W. N. *et al.* NOAA/NSIDC Climate Data Record of Passive Microwave Sea Ice Concentration, Version 3. [1978-2019] (2017). https://nsidc.org/data/G02202/versions/3.

[86] Peng, G., Meier, W. N., Scott, D. J. & Savoie, M. H. A long-term and reproducible passive microwave sea ice concentration data record for climate studies and monitoring. *Earth System Science Data* **5**, 311–318 (2013).

[87] Liston, G. E. *et al.* A Lagrangian Snow-Evolution System for Sea-Ice Applications (SnowModel-LG): Part I—Model Description. *Journal of Geophysical Research: Oceans* **125** (2020).

[88] Stroeve, J. C. *et al.* A Lagrangian Snow Evolution System for Sea Ice Applications (SnowModel-LG): Part II—Analyses. *Journal of Geophysical Research: Oceans* **125** (2020).

[89] Rayner, N. A. *et al.* Global analyses of sea surface temperature, sea ice, and night marine air temperature since the late nineteenth century. *Journal of Geophysical Research* **108**, 4407 (2003). http://doi.wiley.com/10.1029/2002JD002670.

[90] Reynolds, R. W., Rayner, N. A., Smith, T. M., Stokes, D. C. & Wang, W. An improved in situ and satellite SST analysis for climate. *Journal of Climate* **15**, 1609–1625 (2002).